Three-Dimensional Numerical Analysis of Shear Flow Effects on MHD Stability in LHD Plasmas*)

Katsuji ICHIGUCHI[1,2], Yashiro SUZUKI[1,2], Yasushi TODO[1,2], Masahiko SATO[1], Timothée NICOLAS[1], Benjamin A. CARRERAS[3], Satoru SAKAKIBARA[1,2], Yuki TAKEMURA[1], Satoshi OHDACHI[1,2] and Yoshiro NARUSHIMA[1]

[1]*National Institute for Fusion Science, 322-6 Oroshi-cho, Toki 509-5292, Japan*
[2]*SOKENDAI, The Graduate University for Advanced Studies, Toki 509-5292, Japan*
[3]*Universidad Carlos III, 28911 Leganes, Madrid, Spain*

(Received 27 November 2015 / Accepted 25 February 2016)

Effects of poloidal shear flow on the stability of interchange modes in a Large Helical Device (LHD) configuration are numerically studied. Three-dimensional (3D) numerical codes are utilized for the equilibrium and stability calculations. A static equilibrium is employed and a model poloidal flow as a flux function is incorporated in the initial perturbation. The results show that the initially applied flow can suppress the growth of the interchange mode if the flow is sufficiently large.

Keywords: MHD stability, shear flow, 3D numerical simulation, heliotron, interchange mode

DOI: 10.1585/pfr.11.2403035

1. Introduction

In the recent experiments in the Large Helical Device (LHD), a phenomenon similar to a locked mode was observed [1, 2]. In this case, the $m = 1/n = 1$ mode grows rapidly just after the mode rotation stops and causes a partial collapse of the profile in the electron temperature. Here, m and n are the poloidal and toroidal mode numbers, respectively. This phenomenon indicates that the shear flow of the plasma may be a candidate which suppresses the growth of the mode. Thus, we numerically study the effects of the shear flow on the magnetohydrodynamics (MHD) stability against the pressure driven modes in the LHD plasmas by utilizing three-dimensional (3D) numerical codes.

2. Numerical Procedure and Flow Model

In order to investigate the effect of the plasma flow, we should analyze the stability of the equilibrium including the flow consistently. However, any 3D equilibrium calculation scheme consistent with a global flow has not yet been established. Hence, as the first step of this flow stability analysis, we employ a static equilibrium. Then, we set a model global flow in the initial perturbation of the dynamics calculation.

We use the HINT code [3] for the calculation of the static equilibrium. This code solves the equilibrium equations in the cylindrical coordinates (R, ϕ, Z). Here, R and Z are the horizontal and the vertical axes, respectively, and ϕ is the toroidal angle. We use the MIPS code [4] for the stability calculation. This code solves the full MHD equations for the HINT equilibrium in the same cylindrical coordinates. We examine the linear stability and the nonlinear dynamics of perturbations in the equilibrium by following the time evolution of the plasma.

Here, we consider the global flow as a function of the flux surface. In this case, it is convenient to specify the profile of flow components in a flux coordinate system (ρ, θ, ϕ). Here ρ is the label of magnetic flux, and θ is the poloidal angle that is simply determined as $\tan\theta = Z/(R - R_{\rm cnt})$, where $R_{\rm cnt}$ denotes the major radius of the equilibrium magnetic axis. Then, the flow components can be given in the form of $\boldsymbol{V} = (0, V_\theta(\rho), V_\phi(\rho))$ in the coordinates.

Since the MIPS code solves the MHD equations in (R, ϕ, Z), we must obtain the components of $\boldsymbol{V} = (V_R, V_\phi, V_Z)$ at each grid point. By utilizing the relations $\boldsymbol{V} \cdot \nabla P_{\rm eq}(\rho) = 0$ and $V_\theta^2 = V_R^2 + V_Z^2$, we obtain

$$V_R = \frac{1}{A^2}\left[-\frac{1}{R}\frac{\partial P_{\rm eq}}{\partial \phi}\frac{\partial P_{\rm eq}}{\partial R}V_\phi \pm K\frac{\partial P_{\rm eq}}{\partial Z}\right] \tag{1}$$

and

$$V_Z = \frac{1}{A^2}\left[-\frac{1}{R}\frac{\partial P_{\rm eq}}{\partial \phi}\frac{\partial P_{\rm eq}}{\partial Z}V_\phi \mp K\frac{\partial P_{\rm eq}}{\partial R}\right], \tag{2}$$

where

$$\begin{aligned} A^2 &= \left(\frac{\partial P_{\rm eq}}{\partial R}\right)^2 + \left(\frac{\partial P_{\rm eq}}{\partial Z}\right)^2 \text{ and} \\ K &= \left[A^2 V_\theta^2 - \left(\frac{V_\phi}{R}\frac{\partial P_{\rm eq}}{\partial \phi}\right)^2\right]^{1/2}. \end{aligned} \tag{3}$$

author's e-mail: ichiguch@nifs.ac.jp

*) This article is based on the presentation at the 25th International Toki Conference (ITC25).

Here equilibrium pressure P_{eq} is used for the label of the flux instead of ρ. Since V_θ and V_ϕ are given as the functions of ρ, we need to know the relation between the cylindrical and the flux coordinate systems. In order to obtain the relation, we utilize the fact that the input of P_{eq} is given as the function of ρ and the resultant value is obtained as the function of (R, ϕ, Z) in the HINT calculation. By taking the inverse of the function of $P_{eq}(\rho)$ numerically, we obtain $\rho = \rho(P_{eq}(R, \phi, Z))$, which is used for the evaluation of $V_\theta(\rho)$ and $V_\phi(\rho)$ as the function of (R, ϕ, Z).

3. Equilibrium Calculation

We employ the LHD configuration with $R_{ax} = 3.6$ m, $\gamma_c = 1.13$. Here, R_{ax} and γ_c are the horizontal position of the vacuum magnetic axis and the parameter of the aspect ratio of the helical coils, respectively. In the equilibrium calculation, we assume the pressure profile of $P_{eq} = P_0(1-\rho^2)(1-\rho^8)$ and the axis beta of $\beta_0 = 4\%$, where ρ denotes the square root of the normalized toroidal magnetic flux. Figure 1 shows the bird's eye view of this P_{eq}. Figure 2 shows the summary of the equilibrium quantities. The $\iota = 1$ surface is located in the plasma column, where ι is rotational transform. There exists a significant pressure gradient and Mercier stability is unfavorable ($D_I > 0$) at this surface.

We employ the profile of V_θ similar to the experimental result, which is given by

$$V_\theta/V_A = \ln[10(1.1-\rho)]\exp[-9(1-\rho)^2](1-\rho^8). \quad (4)$$

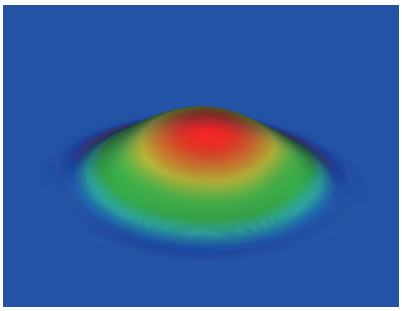

Fig. 1 Bird's eye view of equilibrium pressure profile at the horizontally elongated cross section.

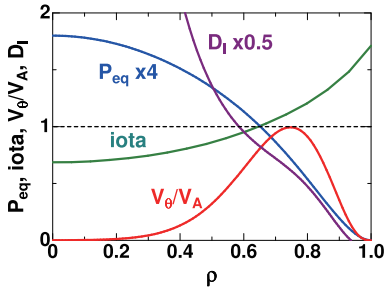

Fig. 2 Profiles of equilibrium pressure, rotational transform, Mercier index, and normalized poloidal flow.

The profile is also plotted in Fig. 2. A substantial shear flow is applied at the $\iota = 1$ surface. Hereafter, we identify the value of the flow by the maximum value of V_θ/V_A, where V_A denotes the Alfvén velocity. We also assume $V_\phi = 0$.

4. Stability Results

In the stability calculation, we add the poloidal shear flow to the input perturbation given by the random noise, and follow the time evolution of the plasma. In the present calculation, we assume the dissipation parameters so that the resistivity, the viscosity, and the perpendicular and the parallel heat conductivities are $\eta/\mu_0 = 10^{-6}$, $\nu = 10^{-5}$, $\kappa_\perp = 10^{-6}$, and $\kappa_\parallel = 10^{-3}$, respectively. Each parameter is normalized by $V_A R_{ax}$. Figure 3 shows the time evolution of the total kinetic energy including the initial flow contribution. At first, we analyze the no flow case $V_\theta/V_A = 0$ as a reference. In this case, an unstable mode grows linearly and is saturated at $t \sim 400\tau_A$, where τ_A denotes the Alfvén time.

Next, we follow the time evolution of the plasma in the cases with $V_\theta/V_A = 10^{-3}$, 10^{-2}, and 10^{-1}. In the case of $V_\theta/V_A = 10^{-3}$, the initial kinetic energy of the flow E_k(flow) is much less than E_{ksat}, where E_{ksat} denotes the saturation level of the kinetic energy in the no flow case. The kinetic energy is constant up to $t \sim 300\tau_A$. This is because the kinetic energy of the flow is much larger than that of the unstable mode in this region. The kinetic energy increases beyond $t \sim 300\tau_A$, and shows almost the same value as that of the no flow case beyond $t \sim 350\tau_A$. In this region, the energy part of the unstable mode in the no flow case is superior to that of the initial flow. Thus, this initial flow is too small to affect the unstable mode.

In the case with $V_\theta/V_A = 10^{-2}$, E_k(flow) is comparable to E_{ksat}. The kinetic energy is almost constant and slightly varies for $t > 400\tau_A$ where the mode in the no flow case is saturated. In the case with $V_\theta/V_A = 10^{-1}$, E_k(flow) is much larger than E_{ksat}. The kinetic energy is constant in the whole time region.

Figure 4 shows the mode pattern of the perturbed pressure $\tilde{P}_{rel}$ at $t = 320\tau_A$, which is defined as $\tilde{P}_{rel} = \tilde{P}/\max(\tilde{P})$, together with the puncture plot of the field lines. In the no flow case, the mode is in the linear phase at

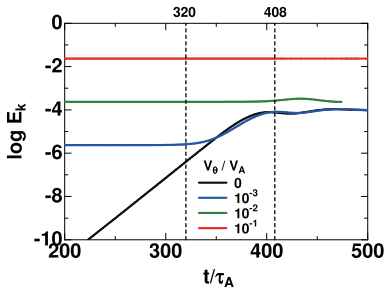

Fig. 3 Time evolution of kinetic energy for $V_\theta/V_A = 0$, 10^{-3}, 10^{-2}, and 10^{-1}.

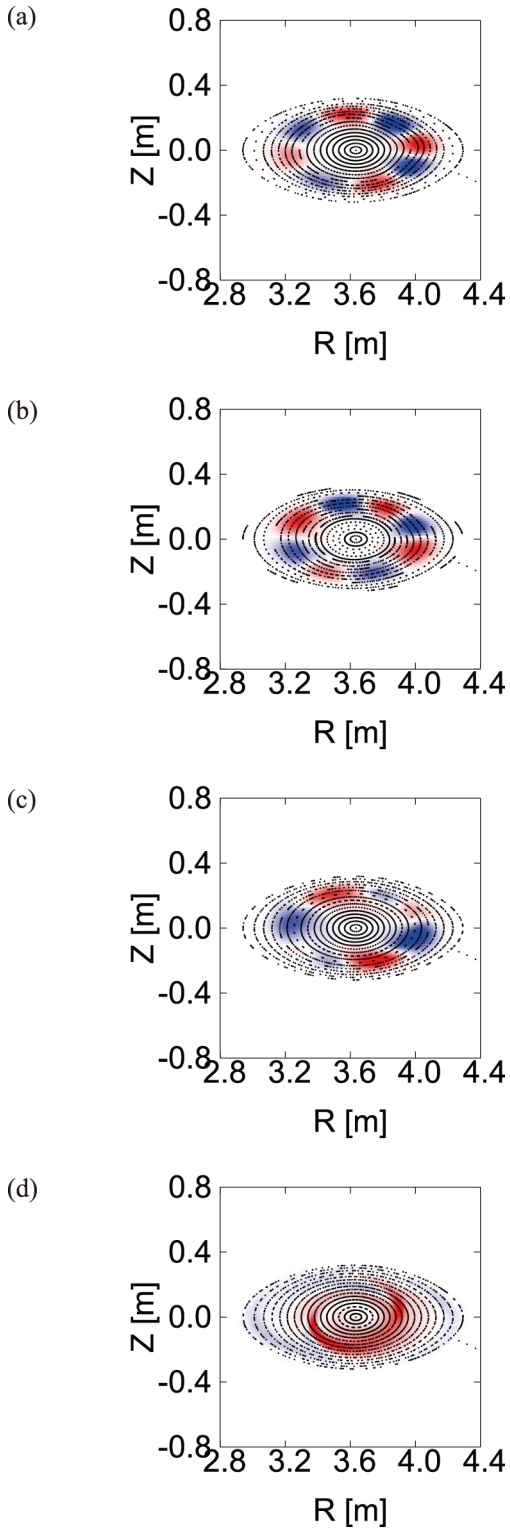

Fig. 4 Mode pattern of perturbed pressure $\tilde{P}_{\rm rel}$ and puncture plots of field lines at $t = 320\tau_{\rm A}$ for (a) $V_\theta/V_{\rm A} = 0$, (b) 10^{-3}, (c) 10^{-2}, and (d) 10^{-1}.

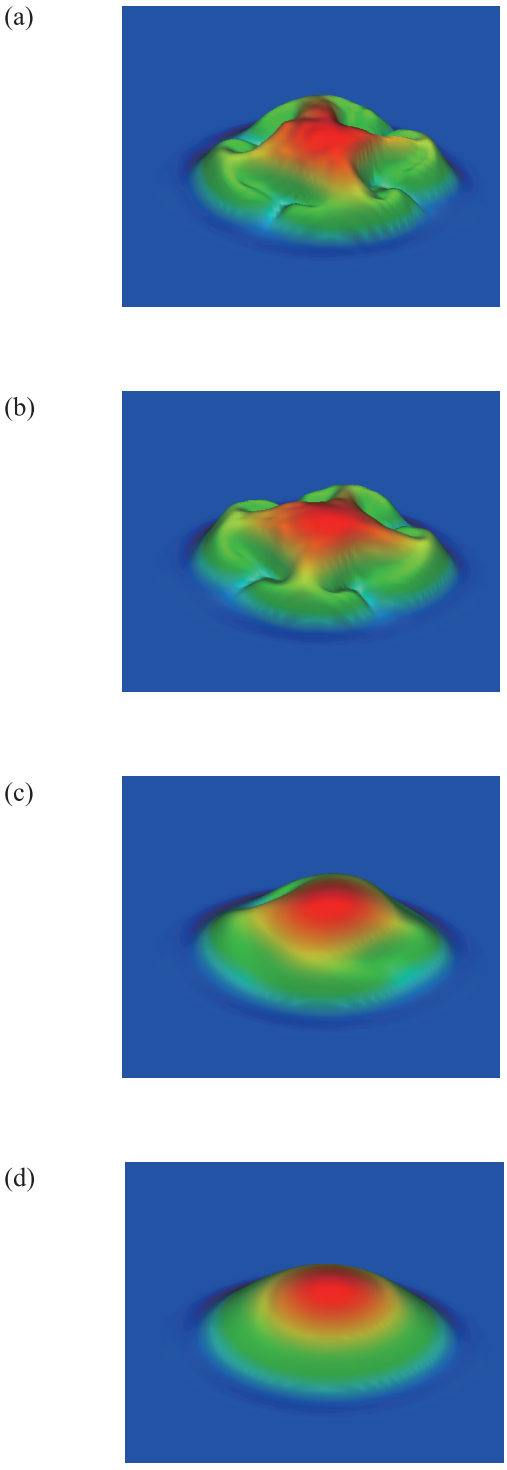

Fig. 5 Bird's eye view of total pressure on horizontally elongated cross section at $t = 408\tau_{\rm A}$ for (a) $V_\theta/V_{\rm A} = 0$, (b) 10^{-3}, (c) 10^{-2}, and (d) 10^{-1}.

this time. The pattern shows the typical interchange mode. The mode numbers of the dominant component are $m = 4$ and $n = 4$, which are determined by the dissipation parameters. In the case of $V_\theta/V_{\rm A} = 10^{-3}$, the mode pattern is almost the same as that of the no flow case. In the case of $V_\theta/V_{\rm A} = 10^{-2}$, the mode number of the dominant mode reduces to $m = 2$. This change of the mode number is similar to that due to the dissipation effects such as viscosity and heat conductivity. In the case of $V_\theta/V_{\rm A} = 10^{-1}$, any explicit mode pattern cannot be recognized.

Figures 5 and 6 show the total pressure and the field line plots with $\tilde{P}_{\rm rel}$ at $t = 408\tau_{\rm A}$ in the saturation phase of the mode. In the no flow case, the pressure profile is

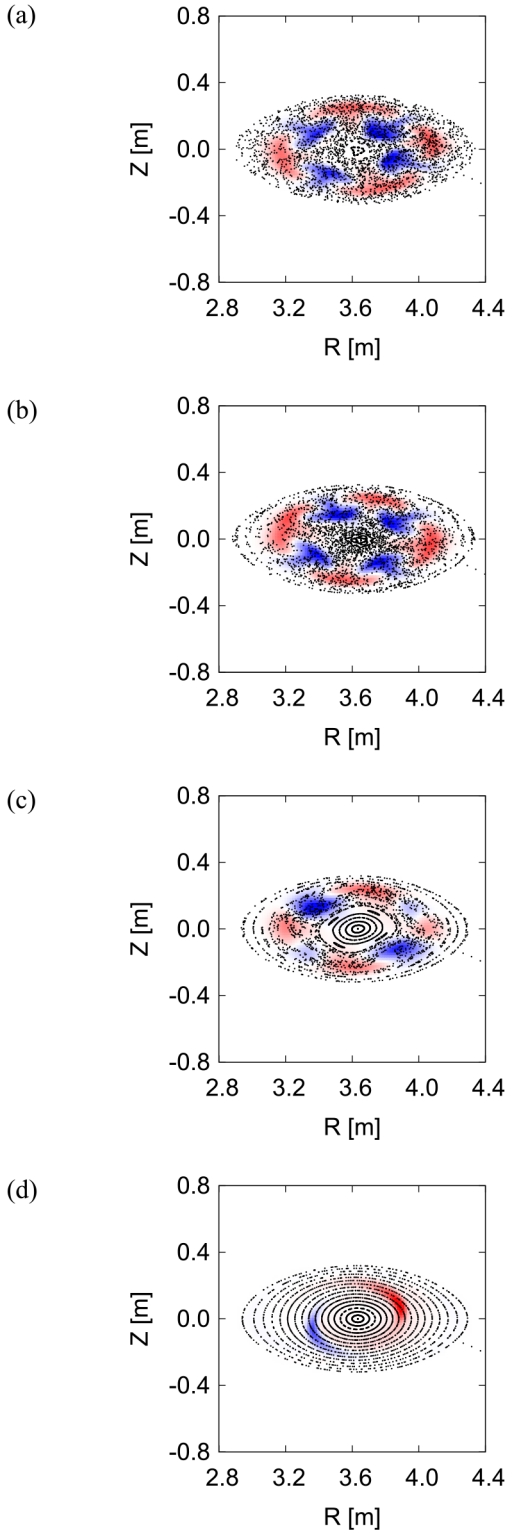

Fig. 6 Mode pattern of $\tilde{P}_{\rm rel}$ and puncture plots of field lines on a horizontally elongated cross section at $t = 408\tau_{\rm A}$ for (a) $V_\theta/V_{\rm A} = 0$, (b) 10^{-3}, (c) 10^{-2}, and (d)10^{-1}.

significantly deformed so as to have $m = 4$ structure and the field lines are stochastic in almost the entire plasma area. In the case of $V_\theta/V_{\rm A} = 10^{-3}$, the behavior is almost the same as that of the no flow case. The deformation of the pressure profile is slightly weaker and the field lines are stochastic except for the peripheral region. In the case of $V_\theta/V_{\rm A} = 10^{-2}$, substantial stabilizing contribution to the mode is seen. The deformation of the total pressure is much smaller than that of the no flow case. In addition, the field lines are stochastic in the limited region. The nested surfaces remain in the wide region except around the surface. Also, the reduction in the mode number from $m = 4$ to $m = 2$ indicates that the global shear flow stabilizes an interchange mode with higher mode numbers more effectively. In this nonlinear evolution, the mode rotation due to the flow is also observed explicitly. In the case of $V_\theta/V_{\rm A} = 10^{-1}$, the stabilizing contribution is further enhanced. No change can be seen in the pressure profile and the flux surfaces also in the nonlinear region.

5. Summary

Effects of poloidal shear flow on the stability of interchange modes in an LHD configuration are studied utilizing 3D numerical codes. Static equilibrium is employed and a model poloidal flow is incorporated in the initial perturbation. The effects of the shear flow are observed as follows:

No flow: The growth of an interchange mode leads to significant pressure collapse and field line stochasticity.

$E_{\rm k}$(flow) $\ll E_{\rm ksat}$: The flow does not interact with the mode in the linear phase and slightly weakens the collapse and the stochasticity.

$E_{\rm k}$(flow) $\sim E_{\rm ksat}$: The flow reduces the mode number and mitigates the collapse and stochasticity.

E_k(flow) $\gg E_{\rm ksat}$: Explicit degradation is not seen in the pressure profile and the magnetic surface structure.

Thus, these results suggest that the initially applied model flow has an effect to suppress the growth of the interchange modes.

The initially applied flow in the present analysis causes the deviation from the force balance of the static equilibrium and induces a plasma motion due to the deviation. Such motion can interact with the growth of the instability. Therefore, the present results does not exactly correspond to the stability property of the steady state with the flow. Nevertheless, the suppression of the mode makes us to expect the stabilizing contribution of the global flow also in the steady state. In order to confirm the stabilizing contribution, we need to obtain the steady state firstly. For this purpose, we can utilize the result obtained with the present scheme, such as the final state of the $V_\theta/V_{\rm A} = 10^{-1}$ case. This analysis is planned as a future study together with the employment of the ExB rotation in modeling the flow.

Acknowledgments

This work is supported by the budget NIFS15KLTT004 of National Institute for Fusion Science (NIFS) and JSPS KAKENHI Grant Number

26-04728 and 15k06651. The super computers Plasma Simulator in NIFS and Helios in the Computational Simulation Center of the International Fusion Energy Research Center (IFERC-CSC) were utilized for the numerical calculations.

[1] Y. Takemura *et al.*, Nucl. Fusion **52**, 102001 (2012).
[2] S. Sakakibara *et al.*, Plasma Phys. Control. Fusion **55**, 014014 (2013).
[3] Y. Suzuki *et al.*, Nucl. Fusion **46**, L19 (2006).
[4] Y. Todo *et al.*, Plasma Fusion Res. **5**, S2062 (2010).